Available online at www.sciencedirect.com
SCIENCE DIRECT®
Environmental Modelling & Software 18 (2003) 231–241
Environmental Modelling & Software
www.elsevier.com/locate/envsoft

Numerical modelling of two-phase flow in a geocentrifuge

B. Ataie-Ashtiani [a,*], S.M. Hassanizadeh [b], O. Oung [c], F.A. Weststrate [c], A. Bezuijen [c]

[a] *Department of Civil Engineering, Sharif University of Technology, Tehran, Iran*
[b] *Centre for Technical Geosciences, and Hydrology and Ecology Section, Delft University of Technology, Delft, The Netherlands*
[c] *Environmental Department, GeoDelft, Delft, The Netherlands*

Received 17 May 2002; received in revised form 22 August 2002; accepted 18 October 2002

Abstract

In this paper, results of DNAPL spreading experiments carried out in a geocentrifuge are analysed. The experiments are performed in the GeoDelft geocentrifuge. The experiments investigate the intrusion of a known amount of PCE into a water-saturated soil sample. They are carried out under 12, 15, and 30*g* conditions. The objectives of these experiments were to assess the potential of geocentrifuge tests for the study of environmental problems, to investigate the effect of acceleration on the spreading of DNAPL, and to determine whether capillary pressure-saturation (P^c–S) curves of soils measured in a geocentrifuge are applicable under 1*g* conditions. In the present paper, numerical simulation is used in the interpretation of the experimental data and for checking the suitability of the designed set-up. Based on these simulations, problems and difficulties regarding the current set-up are explored and suggestions for improvement in the experimental set-up for use in the study of multiphase flow in porous media are presented. We have demonstrated the importance of numerical simulations in the understanding of measured data through scenario analysis and matching numerical and experimental results. Numerical modeling is also shown to be important as an aid in the design of a complex experiment on multiphase flow. Also based on the experimental results and with the use of numerical simulation, we have concluded that the measured P^c–S curve in geocentrifuge is applicable for any practical application at 1*g*.

Keywords: Two-phase flow; Numerical simulation; Geocentrifuge experiment; Porous media; Capillary pressure–saturation curve

1. Introduction

Dense non-aqueous phase liquids (DNAPLs) are among the most common ground-water contaminants and the most difficult to remediate. DNAPLs can reach considerable depths below the water table due to their high density. Moreover, because of their low solubility, once in the subsurface, DNAPLs constitute a long-term source of contamination. Time frames of several decades to centuries have been estimated for a gradual disappearance due to dissolution (Johnson and Pankow, 1992).

The study of DNAPL transport in groundwater requires a correct description of multiphase flow in porous media. This involves a number of material-dependent parameters, including relationships between capillary pressure, saturation, and relative permeability (P^c–S–k^r). These relationships are highly nonlinear and their determination is often a difficult and time-consuming task. Traditional methods of measurement of P^c–S curves requires incremental changes in the imposed capillary pressure, waiting till equilibrium is reached and then measuring equilibrium saturations. This process may take many days to weeks. Recently, attempts have been undertaken to use centrifuges for obtaining P^c–S curves. This is a very quick procedure and a full curve can be obtained within an hour or so.

Geocentrifuges have the ability to increase the body force on the sample and therefore decrease the required testing time. In recent years, the use of geocentrifuge for environmental studies has greatly increased. In particular, slow transport processes have been studied within a geocentrifuge. Examples are the transport of solutes within saturated (low-permeable) media (cf. Zimmie and Mahmoud, 1995; Nakajima et al., 1998; Zimmie and Mahmud, 1995) or, within unsaturated zone (cf. Griffioen and Barry, 1998; Basha and Mina, 1999; Depountis

* Corresponding author.
E-mail address: ataie@sina.sharif.ac.ir (B. Ataie-Ashtiani).

1364-8152/03/$ - see front matter © 2003 Elsevier Science Ltd. All rights reserved.
doi:10.1016/S1364-8152(02)00092-0

et al., 2001), obtaining capillary pressure and/or relative permeability curves for multiphase flow (cf. Ayappa et al., 1994; Ali and Barrufet, 2001; Zhiang and Ruth, 1999; Baldwin and Spinler, 1998), simulation of spreading of LNAPL (cf. Knight and Mitchell, 1996; Illangasekare et al., 1991; Mitchell and Stratton, 1994) and DNAPL (cf. Garnier et al., 1998; Pantazidou et al., 2000), simulation of coupled thermo-hydro-mechanical effects (cf. Vaziri, 1996) and air sparging (Marulanda et al., 2000). Mitchell (1998) has provided an extensive review of the use of centrifuge for geoenvironmental practice and education.

One of the largest geocentrifuge facilities in the world is located at GeoDelft, Delft, The Netherlands. The arm of the centrifuge is 6 m long and an acceleration of 300g can be reached. Characteristics of the GeoDelft geocentrifuge have been described by Nelissen (1991). Recently, a series of experiments have been carried out in this geocentrifuge in the framework of the EU-project NECER (Network of European Centrifuges for Environmental Geotechnic Research). The objectives of these experiments were to investigate the potential of geocentrifuge tests for the study of environmental problems, to investigate the effect of acceleration on the spreading of DNAPL, and to determine whether P^c–S curves of soils measured in a geocentrifuge are valid under 1g . To the authors' knowledge, this is the first time that a geocentrifuge has been used for obtaining P^c–S curves for a DNAPL-water system.

The purpose of this paper is to present our efforts in modelling the experimental results, to address the objectives described above, and to show how the modelling work is used to investigate relevant physical processes and to identify possible shortcomings of the experimental design. It appeared that the simulation of the geocentrifuge experiments was not a straightforward task. This was because essential data on boundary conditions were not available and measurements of pressure transducers needed to be properly interpreted before they could be used. Thus, in this work we had to make educated guesses and use expert judgment in setting up our simulation work. The simulation procedure and scenarios developed have helped us to gain insight into the physical processes involved in geocentrifuge experiments and have made it possible to interpret the results properly. Based on these simulations, problems and shortcomings of the current set-up are explored and suggestions for its improvement are made. The main focus of this work is to show that the measurement of constitutive relationships rapidly obtained by the geocentrifuge experiments at a higher g-level is suitable for modeling in normal gravity.

Experimental setup and results are presented briefly in Section 2. The numerical simulations are conducted with the water–oil mode of multi-fluid flow simulator STOMP (White and Oostrom, 1997). Processes modeled in STOMP and its numerical features are described in Section 3. In Section 4 results of one-dimensional simulation with and without modification for boundary effects are given. In Section 5, the applicability of constitutive relationships of two-phase flow measured in a geocentrifuge to 1g conditions is discussed. Finally, conclusions are presented in Section 6.

2. Experimental set-up and results

Here, a brief description of the experimental set-up is given; further details can be found in Oung et al. (2000a, b). Schematic presentation of the column set-up is shown in Fig. 1. In these experiments, the displacement of water by PCE and its subsequent displacement by water in a column are studied. It is a 10-cm cylinder consisting of three parts: the inflow reservoir, a soil compartment and the PCE collection reservoir. Displaced water from the PCE collection reservoir may flow over to the water collection reservoir (see Fig. 1). The whole system is placed in the geocentrifuge container. As the geocentrifuge reaches its designated maximum speed, the container tilts horizontally until the column assumes an almost horizontal position and the desired g-level is reached at the soil sample surface (position of PPT1 transducer in Fig. 1).

Instrumentation of the set-up consisted of a combination of hydrophobic pore pressure transducers (PPTs) and tethra probe frequency domain sensors (TPs) for

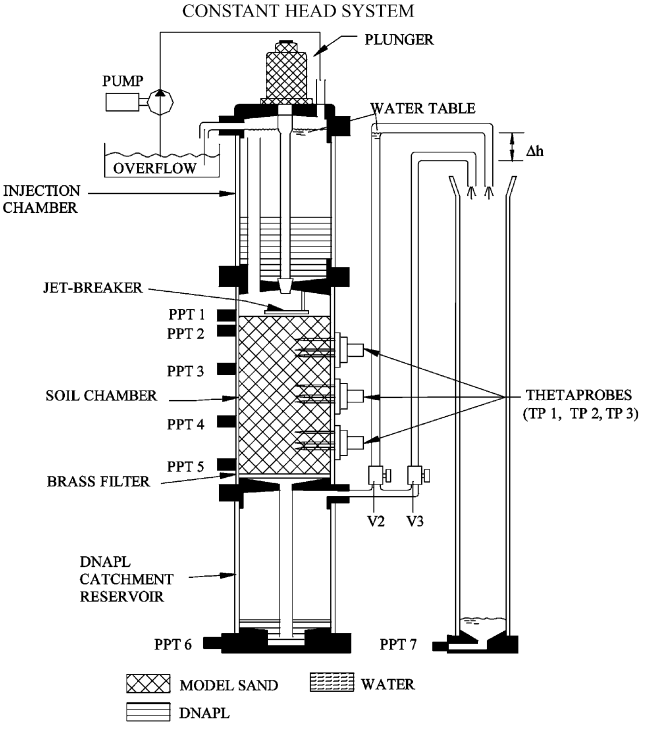

Fig. 1. Sketch of the test column used in centrifuge experiments.

measuring water saturation. There are seven PPTs and three TPs. The positions of the transducers, measured from the bottom of the DNAPL collection reservoir, are given in Table 1. PPT7, at the bottom of the water collection reservoir, was used to determine cumulative outflow of water, as explained later. The water level in the inflow reservoir was kept constant at 59.3 cm.

There are three valves: V1, V2 and V3. V1 is actually a plunger, which is hydraulically controlled. V2 and V3 are electromagnetic valves. V2 controls the commencement of flow through the column. V3 allows the maintaining of a 2-cm head difference between inflow and collection reservoirs. This valve was not used in these experiments. The experiment starts by opening valve V1. PCE replaces water in the inflow reservoir and comes into contact with the soil surface. Excess water escapes via the top overflow (see Fig. 1). Flow of PCE through the soil starts by opening valve V2. Although the water level in the pipe V2 is the same as in the inflow reservoir, flow through the soil column occurs because PCE is heavier than water.

The Zeijen sand was used in these series of experiments. Zeijen sand is prepared by washing, drying and sieving out the organic matter and the very fine grained material. The grain size distribution is fairly uniform with D_{15} = 0.06 and D_{50} = 0.085 mm for Zeijen sand. Sand is poured into the column under water and the column is tapped in order to reach 100% relative density under fully saturated conditions. The sand column length is 18 cm.

The column test was designed to ensure a one-dimensional flow pattern. Initially, 1 liter of perchloroethylene (PCE) is injected in the inflow reservoir. In order to visualise PCE flow and to facilitate the measurement of the residual saturation later on, PCE is dyed with Sudan Red (0.16 g/l of PCE).

Pertinent sand properties, including permeability and Brooks–Corey (1964) parameters are listed in Table 2. The parameters were obtained by static measurement of capillary-pressure–saturation curves under quasi-static conditions (Oung and Bezuijen, 2001). The geocentrifuge test proceeded in the following operational order. The geocentrifuge was spun up to establish the desired *g*-level. Valve V1 was opened and PCE reached the sand surface. Valve V2 was opened and PCE started to infiltrate the sand column. After all mobile PCE had left the column, valve V2 was closed and geocentrifuge was brought to a halt. In this series of experiments, three different acceleration levels, namely 12, 15, and 30*g*, were applied.

Table 2
Sand and fluid properties

Property	Units	Zeijen sand
Permeability, k	[m^2]	3.0×10^{-12}
Porosity, n	[-]	0.375
Entry pressure, p_d	[m]	0.56
Pore size distribution index, λ	[-]	6.3
Residual saturation, S_r	[-]	0.134
PCE density	[kg/m^3]	1623
PCE viscosity	[Pa s]	3.15×10^{-4}
PCE–water interfacial tension	[N/m]	44.4×10^{-3}

The responses of PPT1–PPT5 sensors for the case of Zeijen sand at 15*g* are presented in Fig. 2. As all systems were below the water level, hydrostatic water pressure was subtracted from the raw signals of all PPTs. All pressure transducers were tested and calibrated before installation. However, there is always some shift in the readings of the pore pressure gauges. This is caused by forces on the pore pressure gauge due to their mounting and to the increased *g*-level during spinning up. It is therefore common practice to try to start an experiment with a well-defined pressure distribution. This was also done in these experiments. The hydrostatic pressure before the release of the DNAPL was used as a starting point. Thus, the correction of PPT readings for hydrostatic pressure also accounts for pressure shifts due to the mounting and the increased *g*-level.

As pressure transducers were hydrophobic, i.e. they

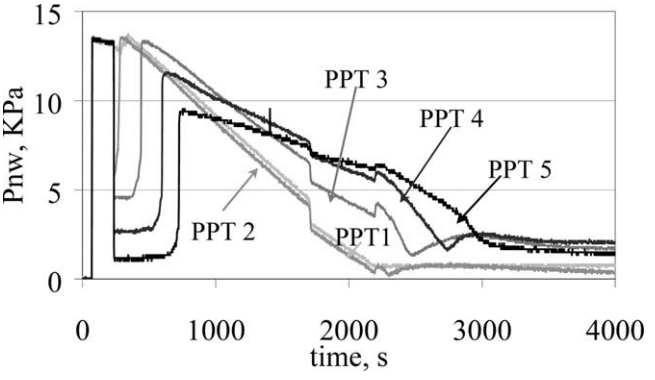

Fig. 2. Pressure measured at PPT1 to PPT5, after subtraction of hydrostatic water pressure.

Table 1
Heights of transducers from the bottom of collection chamber

Sensors	PPT1	PPT2	TP1	PPT3	TP2	PPT4	TP3	PPT5	PPT6
Positions (cm)	38.2	37.2	35.0	32.2	29.6	26.2	24.0	21.2	1.35

measured the non-wetting phase pressure, P_{nw}, once mobile PCE reached them. Before that, they measured water pressure. After the passage of PCE, however, they are in contact with a mix of water and residual PCE and therefore, that reading does not represent any of the pressures as seen in Fig. 2.

Based on readings of the PPT1 sensor, located just below the sand surface, one can conclude that PCE infiltration is completed at $t = 2190$ s, when PPT1 shows no changes in readings anymore. Later in this paper, this observation will be used in the definition of the top boundary condition in the numerical model. A sharp drop in all pressure readings is observed at about 1720 s. This marks the passing of the free PCE surface through the injection valve V1. Because the valve has a small opening, there is a very quick pressure drop as the PCE passes through this opening.

Fig. 3 shows water saturation measured by TP sensors. Obviously, in this experiment the column undergoes a stage of water drainage when PCE floods in and a stage of water inhibition as PCE leaves the sand. The hysteresis effects have not been included in the numerical simulations because the purpose of these simulations is to capture the general trend of physical process rather than matching all details.

3. Numerical model

The two-phase flow simulations are carried out using the simulation package STOMP (Subsurface Transport Over Multiple Phases). STOMP is a package consisting of 11 modes for simulation of non-isothermal multiphase flow and multi-component transport in a heterogeneous medium in three dimensions. This fully implicit, integrated finite difference code has been used to simulate a variety of multi-fluid systems (Oostrom and Lenhard, 1998; Schroth et al., 1998; Oostrom et al., 1997; Ataie-Ashtiani et al., 2001, 2002). The simulations discussed in this paper were conducted with a non-hysteretic two-phase version of the water–oil mode of STOMP. In this mode, the following mass balance equations for the phases water (superscript w) and oil (superscript o) are solved:

$$\frac{\partial}{\partial t}(n\rho_\gamma S_\gamma) = -\nabla\cdot\mathbf{q}_\gamma \quad \text{for } \gamma = \text{w, nw} \tag{1}$$

where

$$\mathbf{q}_\lambda = -\frac{\rho_\gamma k_{r\gamma}\mathbf{k}}{\mu_\gamma}(\nabla P_\gamma + \rho_\gamma g\mathbf{e}_g) \quad \text{for} \quad \gamma = \text{w, nw} \tag{2}$$

In these equations, subscripts γ may be w for water phase or nw for nonaqueous (oil) phase, n is porosity, ρ is density (M L^{-3}), S is saturation, q is the fluid mass flux (M L^{-2} T^{-1}), k_r is relative permeability, k is the intrinsic permeability tensor (l^2), μ is viscosity (M L^{-1} T^{-1}), P is pressure (M L^{-1} T^{-2}), g is the magnitude of gravitational acceleration (L T^{-2}), and $\mathbf{e}_g$ is the unit vector in the vertical direction.

In addition to the well-known van Genuchten (1980) and Brooks and Corey (1964) capillary pressure–saturation relations, this version of the simulator also allows for tabular input of fluid saturations and pressures. Relative permeability–saturation relations are interpolated from tabular input or computed based on either the Burdine (1954) or Mualem (1976) pore-size distribution model. In the present article, the Brooks–Corey formula for capillary pressure is used:

$$S_e = \left(\frac{P^c}{P_d}\right)^{-\lambda} \quad \text{for } P^C \geq P_d \tag{3}$$

where

$$S_e = \left(\frac{S - S_r}{1 - S_r}\right), \quad 0 \leq S_e \leq 1 \tag{4}$$

In these equations, P^c is capillary pressure (M l^{-1} T^{-2}), P_d is entry pressure (M l^{-1} T^{-2}), S_e is effective saturation, S^r is irreducible water saturation, and λ is the pore size distribution index.

The relative permeability of the medium to the aqueous phase, k_{rw}, and nonaqueous phase, k_{rn}, are given by the Burdine formula:

$$k_{rw} = S_e^{[(2+3\lambda)/\lambda]} \tag{5}$$

$$k_{rn} = (1 - S_e)^2(1 - S_e^{[(2+\lambda)/\lambda]}) \tag{6}$$

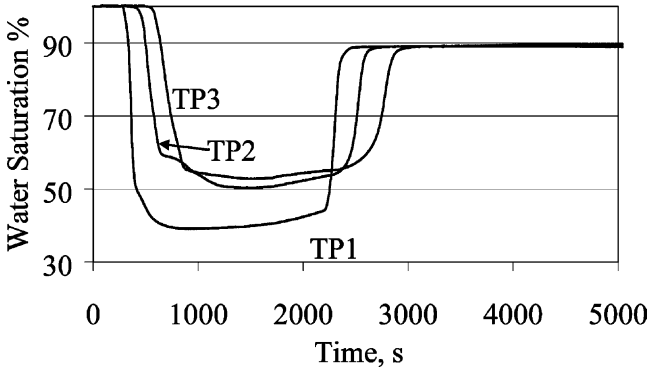

Fig. 3. Measured water saturation at TP1 to TP3.

4. Numerical simulations

In this section, the multi-phase flow in the test column is conceptualized to be one-dimensional. The case of Zeijen sand at 15g is described first. The procedure for other cases is similar. Properties of the Zeijen sand, including permeability and Brooks–Corey parameters as well as fluid properties are listed in Table 2. Relative permeability–saturation relations were computed based on the Burdine (1954) pore-size distribution model.

The boundary conditions at the top and bottom of the sand column and their variations with time are given in Fig. 4. The DNAPL pressure at the top of column is based on the PPT1 reading. Fig. 4a shows how the pressure readings at PPT1 are approximated for application as P_{nw} boundary condition. At the same time, a no-flux boundary condition is imposed for water. When PPT1 readings indicate that there is no PCE left (at time t = 2190 s), the top boundary condition is changed to a specified water pressure for water and no-flux boundary condition for PCE. The water pressure at this time is calculated based on the water level of the inflow reservoir. The water and PCE pressures at the bottom boundary are assumed to be equal (i.e. zero capillary pressure) and are based on the free water surface in the flow line containing valve V2. The initial condition is calculated based on the level of water and PCE in the inflow reservoir.

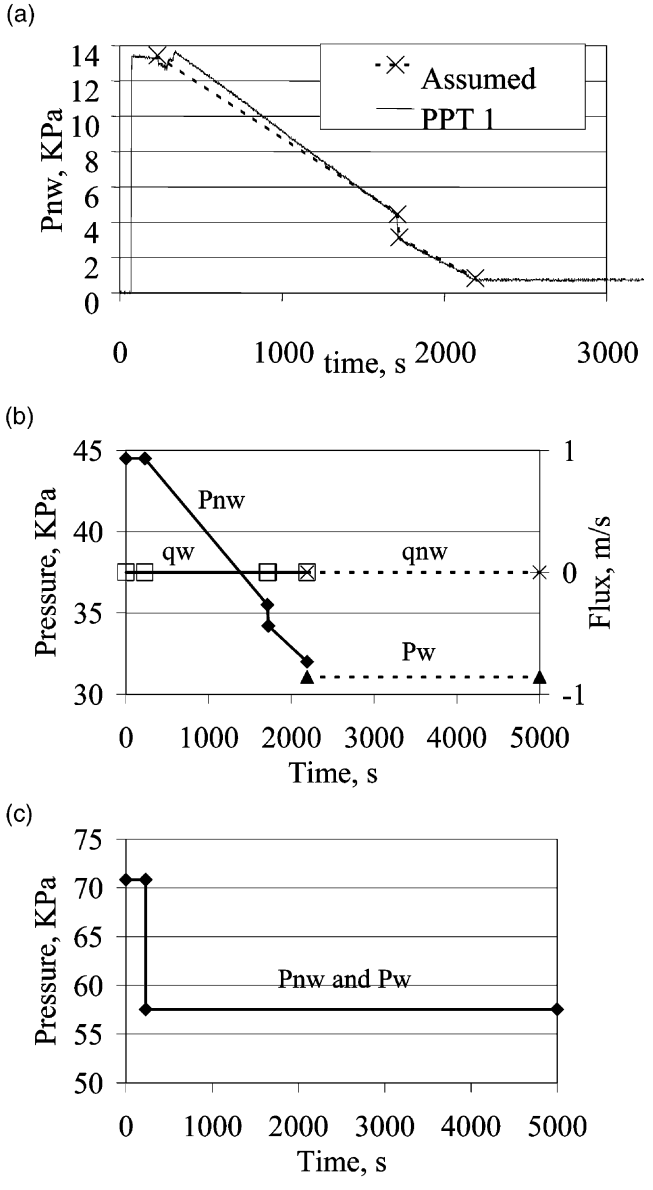

Fig. 4. (a) Approximation of P_{nw} readings at PPT1, (b) boundary conditions at the top of sand column, (c) boundary condition at the bottom of sand column.

The soil column is discretized into a one-dimensional grid with a constant nodal spacing of 2.5 mm. The time step varies automatically from 1-10 s. Comparisons of simulation results and experimental data are shown in Fig. 5. Water saturation plots are shown in Fig. 5a–c. There is a reasonable agreement between measured and calculated values. In Fig. 5d, calculated and measured values of PCE outflow volumes (NW_{out} and $EXP.NW_{out}$, respectively), water outflow volumes (W_{out} and $EXP.W_{out}$) as well as calculated values of inflow water and PCE volumes (W_{in} and NW_{in}, respectively) are shown. Here, there are considerable discrepancies between calculated and measured outflux volumes. Finally, pressure curves at PPT3 and PPT5 are shown in Fig. 5e and f, respectively. While the result of simulation for PPT3 (at least the trend) is somewhat acceptable, the calculated pressure curve at PPT5 (near the bottom boundary) is completely different from the measured curve. Also, the total PCE influx volume was 1 liter whereas the calculated value is 1.40; thus 40% more.

To explain these discrepancies, a sensitivity analysis with respect to the parameters of the P^c–S_w relationship was performed. Table 3 gives seven sets of parameter combinations used here. The base set (set 1) was constructed using a method proposed by Kueper and Frind (1991) which is based on the Leverett (1941) function. The other sets were produced by an increase or decrease of 50% or a decrease of 33% in the base value of the parameter of interest.

Table 4 gives the calculated influx and outflow volumes of PCE at 4000 s based on different parameter sets for different cases after 4000 s. The measured values of these quantities are 1.0 and 0.89 liters, respectively. As seen, a better agreement for the volume of PCE influx and outflow can be obtained by increasing entry pressure (case 2) or decreasing pore distribution coefficient (case 5). In all other cases, the fluxes are overestimated.

Fig. 6 shows the PCE pressure, P_{nw}, at PPT5 for the seven cases. As seen, the declining trend, which is observed in the experimental results, cannot be reproduced by changing the P^c–S_w curve parameters. Although, in the case of high entry pressure (6.0 kPa), the value of P_{nw} calculated numerically has increased in comparison to other cases, still it shows a different trend in comparison to the experimental data. Therefore, the differences between numerical and experimental results cannot be explained by variation in the material characteristics.

Obviously, it is not possible to measure all quantities at all points of interest, due to budget constraints and, more importantly, practical restrictions. However,

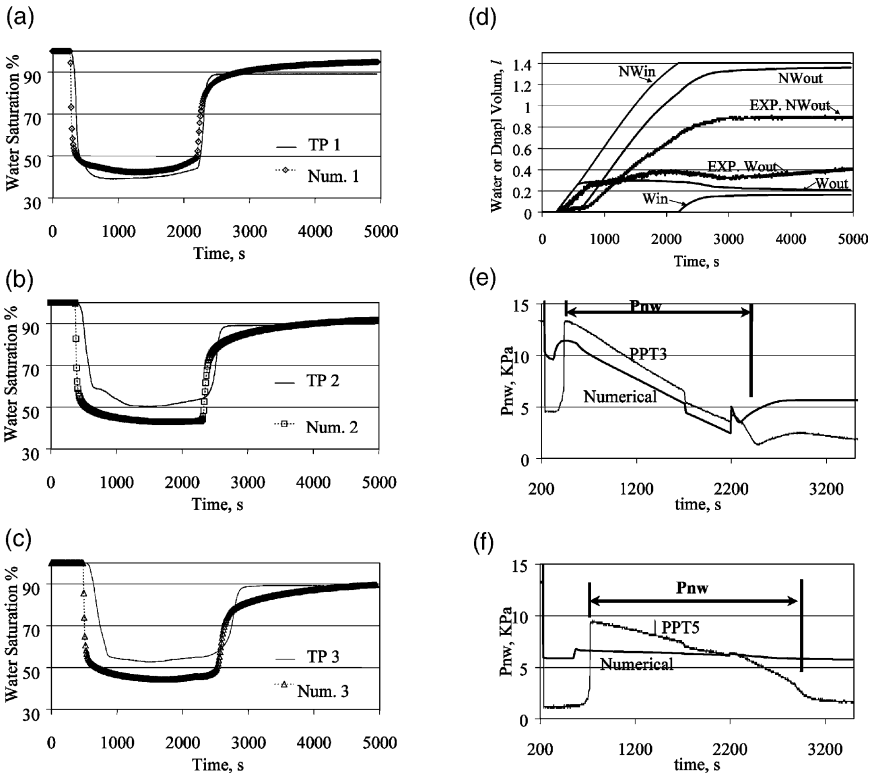

Fig. 5. Experimental and numerical results at 15*g* of (a) water saturation at TP1, (b) water saturation at TP2, (c) water saturation at TP3, (d) accumulated volume of PCE and water inflow and outflow, (e) PCE pressure at PPT3, and (f) PCE pressure at PPT5.

Table 3
Seven sets of parameter values for sensitivity analysis

	1	2	3	4	5	6	7
Pd, kPa	4.0	6.0	2.7	4.0	4.0	4.0	4.0
λ	2.48	2.48	2.48	3.72	1.65	2.48	2.48
Swr	0.078	0.078	0.078	0.078	0.078	0.117	0.052

Table 4
Volume of PCE influx and outflow after 4000 s

	1	2	3	4	5	6	7
PCE influx volume, l	1.41	0.80	1.80	1.59	1.18	1.43	1.40
PCE outflow volume, l	1.36	0.75	1.75	1.53	1.13	1.38	1.35

numerical simulation assists to fill the gaps in the available measured data.

As it was shown in Fig. 5, the agreement of numerical with experimental results for P_{nw} deteriorated at positions closer to the bottom of the sand column. This trend pointed to the possibility that the boundary condition may be inconsistent with the actual situation. The bottom boundary condition imposed here was that fluids might flow out freely into the collection reservoir, at zero capillary pressure. The water and PCE pressures at the bottom boundary were assumed to be equal (i.e. zero capillary pressure) and were based on the free water surface in the flow line containing valve V2. However, head measurements in the DNAPL collection reservoir and in the flow lines behind valve V2 show that there is a considerable pressure drop in the flow line. This might be due to flow resistance caused by regulation valve V2 and other frictional effects. In order to include such effects, another set of simulations was performed as described below.

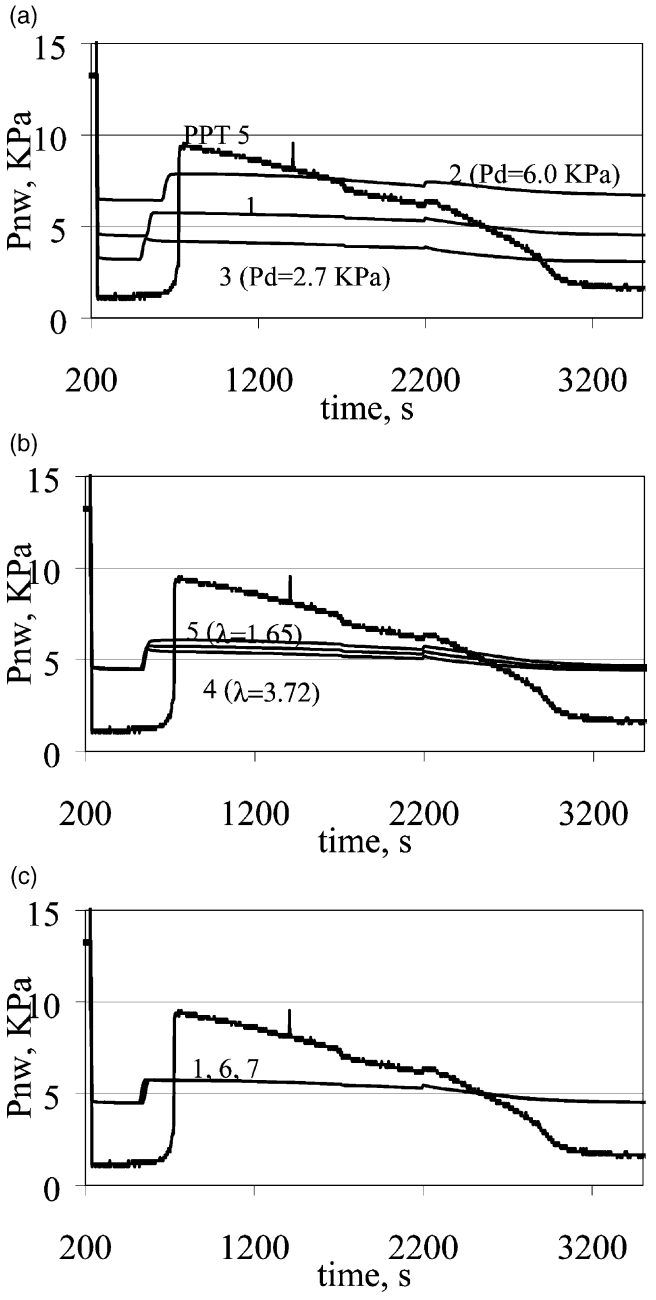

Fig. 6. The P_{nw} at PPT5 for various cases presented in Table 3: (a) variation in entry pressure, (b) variation in pore distribution index, and (c) variation in residual saturation of water. Case numbers are shown.

The resistance to flow is simulated by adding a virtual layer of porous medium to the bottom of the sample with a lower intrinsic permeability and a lower entry pressure. The lower entry pressure is chosen because this layer is not supposed to be a barrier to the flow of DNAPL. For the same reason, relative permeabilities of the bottom layer for both phases (water and PCE) are assumed to equal 1 at all times (not a function of saturation).

A large number of simulations with various combinations of intrinsic permeability and entry pressure were performed. The best results were obtained for the case when the bottom porous medium was chosen to be 2.5 mm thick with a permeability 50 times smaller and an entry pressure 10 times smaller than the sample. The results are shown in Fig. 7. It is evident that improved simulation results are obtained. The simulated and measured values of PCE outflow volumes (curves NW_{out} and $EXP.NW_{out}$, in Fig. 8d, respectively), water outflow volumes (curves W_{out} and $EXP.W_{out}$, respectively) are quite close in this case. Also, the calculated volume of inflow PCE (curve NWin) approaches 1 liter which is the amount that was infiltrated in the experiment.

Obviously, this conceptualization of bottom boundary effects on the water and PCE movement is just a very rough approximation of reality. It is not clear how this resistance changes in time depending on the outflux of water and PCE. Commonly, the head loss in a pipe is assumed to be proportional to the square of velocity. The pressure loss cannot be exactly formulated and implemented in this problem. By adding a layer of porous medium to the bottom where Darcy's law applies, we effectively assume that the pressure loss in each phase is proportional to flux of that phase in the bottom of the sample. Nevertheless, numerical results show that this conceptualization has been successful to a large extent.

Based on these numerical analyses, for any further experiments, the bottom arrangement should be modified so as to have a controlled boundary condition for water and DNAPL flow. Also, to increase the accuracy of simulations, a more controlled boundary condition at the top of the sand column would be desirable. For example, maintaining a constant DNAPL-level will lead to having only drainage and thus avoids hysteretic conditions. Accurate measurement of water pressure along the sand column is a necessity for any detailed study of phenomena like dynamic effects and effects of micro-heterogeneities on P^c–S–k^r. Therefore, pressure transducers for water pressure measurement should be installed.

5. Geocentrifuge application for measurement of constitutive relationships of two-phase flow

In spite of shortcomings of the data collected in these experiments, we believe they can provide insight into the utility of geocentrifuge experiments for obtaining two-phase constitutive relationships. We try to reach such a conclusion by induction. We use the same P^c–S curve for simulating various experiments carried out at different g-levels. If we obtain satisfactory agreement with measurements, then we conclude that the measurement of the P^c–S curve at a higher g-level in a geocentrifuge can be used for 1g simulations.

Figs. 8 and 9, respectively, present the results of 12 and 30g experiments and simulations without and with the effect of bottom resistance. As seen in these figures,

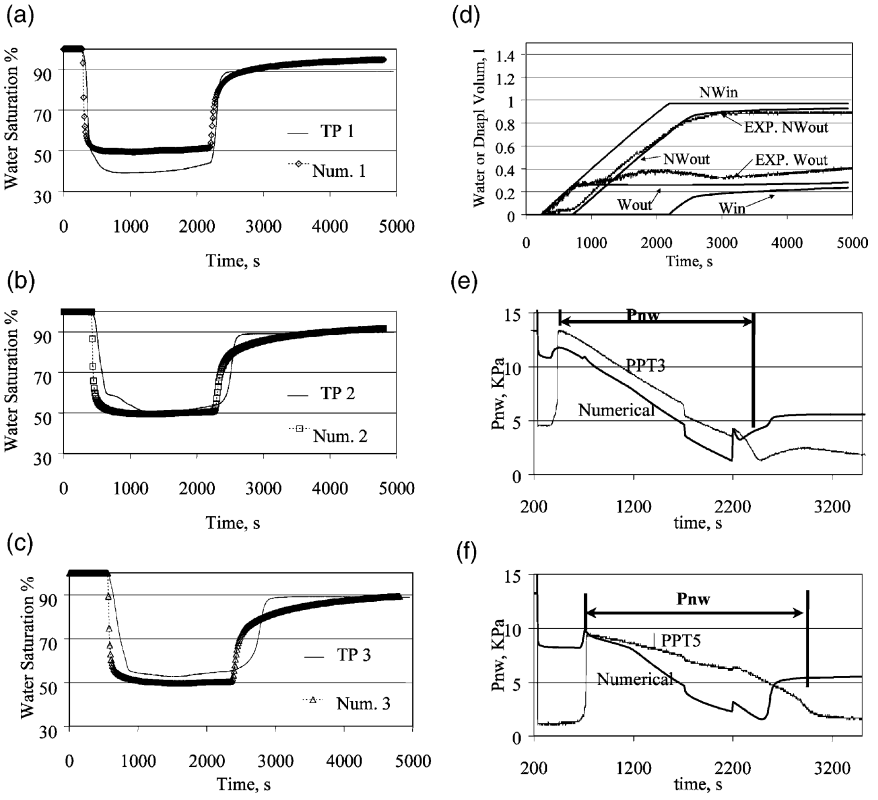

Fig. 7. Experimental and modified numerical results at 15*g* of (a) water saturation at TP1, (b) water saturation at TP2, (c) water saturation at TP3, (d) accumulated volume of PCE and water inflow and outflow, (e) PCE pressure at PPT3, and (f) PCE pressure at PPT5.

with the same P^c–S curve and imposed boundary condition, the general behavior of PCE movement has been reproduced in the numerical simulations. The calculated saturation–time curves are similar to experimental results and also the total amount of PCE entering the sample, 1 liter, is reproduced well by numerical simulations. It should be noted that because of malfunctioning of PPT6 and PPT7 sensors in these cases, the correct values of the water and PCE outflow fluxes from the experimental data could not be obtained. Numerical simulation results for outflow fluxes of water and PCE are reasonable. Also, the pressure measurement is simulated reasonably well for all *g*-levels.

Overall, the agreement between the numerical model and experimental data is reasonably good, considering the fact that in the numerical simulation secondary processes like hysteresis and non-wetting phase entrapment have not been included. We know that entrapment is happening in these experiment as about 15% of PCE remained behind in the sample. Also, the bottom boundary condition in these experiments is not very well controlled and it cannot be exactly simulated. The effect of this boundary condition, however, has been roughly included in the model. Thus, based on these results, it can be concluded that the P^c–S curve measured in geocentrifuge is valid for practical applications under 1*g*. This means that the capillary pressure measured in the geocentrifuge is independent of the acceleration (*g*-level). A similar result for unsaturated flow is obtained by Depountis et al. (2001). They found that the height of capillary rise is inversely proportional to N (the ratio of centrifugal acceleration to gravity). Given the fact that the weight (centrifugal force) is directly proportional to N, we can easily establish that capillary pressure is independent of the *g*-level.

Obviously, further investigations with an improved experimental set-up and procedure, are required to reveal the significance of the secondary effects mentioned above.

6. Summary and conclusions

A series of two-phase flow experiments have been performed in the GeoDelft geocentrifuge facility in order to study DNAPL spreading in porous medium. The experiments constituted the intrusion of a known amount of PCE into a water saturated soil sample. They were carried out under 12, 15, and 30*g*. The experimental program was designed with the main goal of obtaining detailed quantitative data to study the spreading of DNAPL under various *g*-levels and to address scale problem in geocentrifuge experiments.

In this work, a numerical model was employed for the

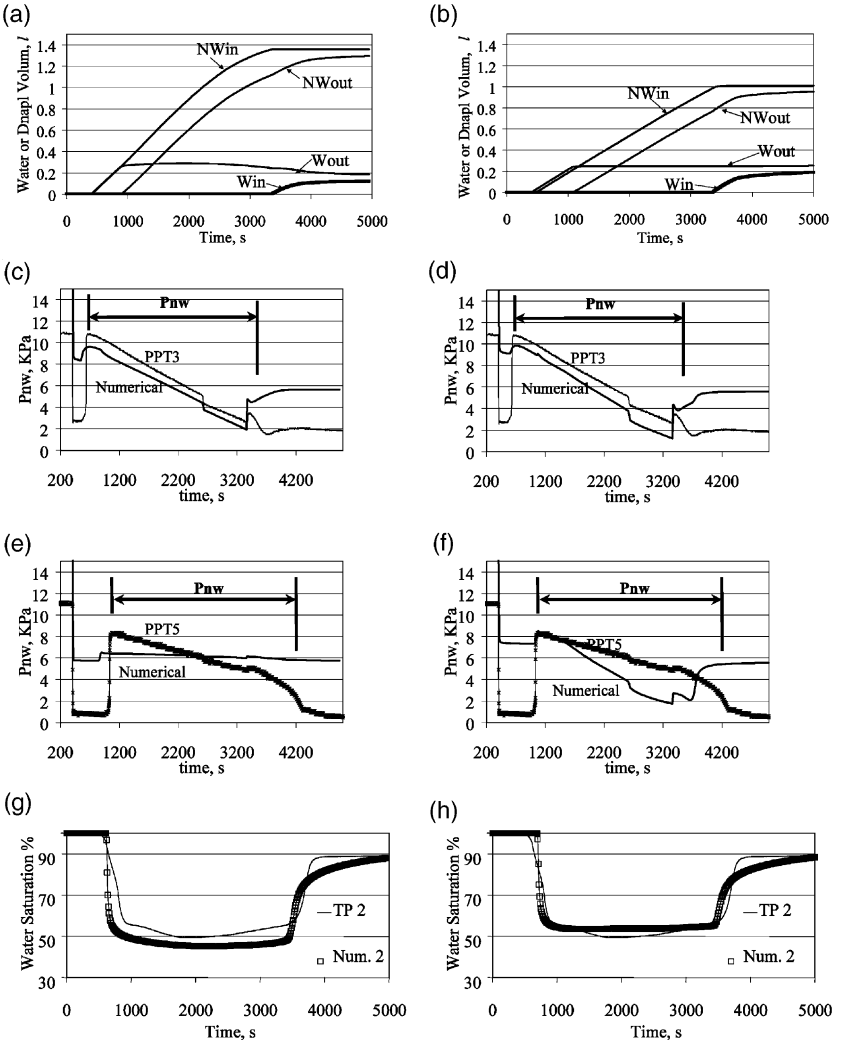

Fig. 8. Experimental and numerical results at 12*g* of (a) accumulated volume of PCE and water inflow and outflow, (b) accumulated volume of PCE and water inflow and outflow for modified simulation, (c) PCE pressure at PPT3, (d) PCE pressure at PPT3 for modified simulation, (e) PCE pressure at PPT5 and (f) PCE pressure at PPT5 for modified simulation, (g) water saturation at TP2, and (h) water saturation at TP2 for modified simulation.

interpretation of the experimental data. Based on these simulations, problems and difficulties regarding the current set-up were explored. Numerical simulations indicated that some of the features observed in collected data are due to uncertainties in defining the bottom boundary condition. This boundary was simulated as a virtual layer added to the bottom of the modeling domain. This layer had a lower permeability and a lower entry pressure than the sample.

In spite of shortcomings in the experimental data, and given the fact that in the numerical simulation secondary processes like hysteresis and non-wetting phase entrapment were not included, we have been able to simulate experimental data reasonably well. All in all, by reproducing the experimental results of different *g*-levels using a unique constitutive relationship measured under 1*g*, it can be concluded that the measured P^c–S curve in geocentrifuge is valid for any practical application at 1*g*. The common practice in almost all field-scale studies, or even laboratory studies, is that these secondary processes are not included. Nevertheless, further investigations with modifications in the experimental set-up and procedure are required to reveal the significance of these secondary effects.

Acknowledgements

This research has been carried out in the framework of the TRIAS Project “Upscaling micro-heterogeneities in two-phase flow in porous media” (Delft Cluster Project no. 5.3.1). The European Commission sponsored the experimental part of this research as a part of the project NECER (Network of European Centrifuges for Environmental Research).

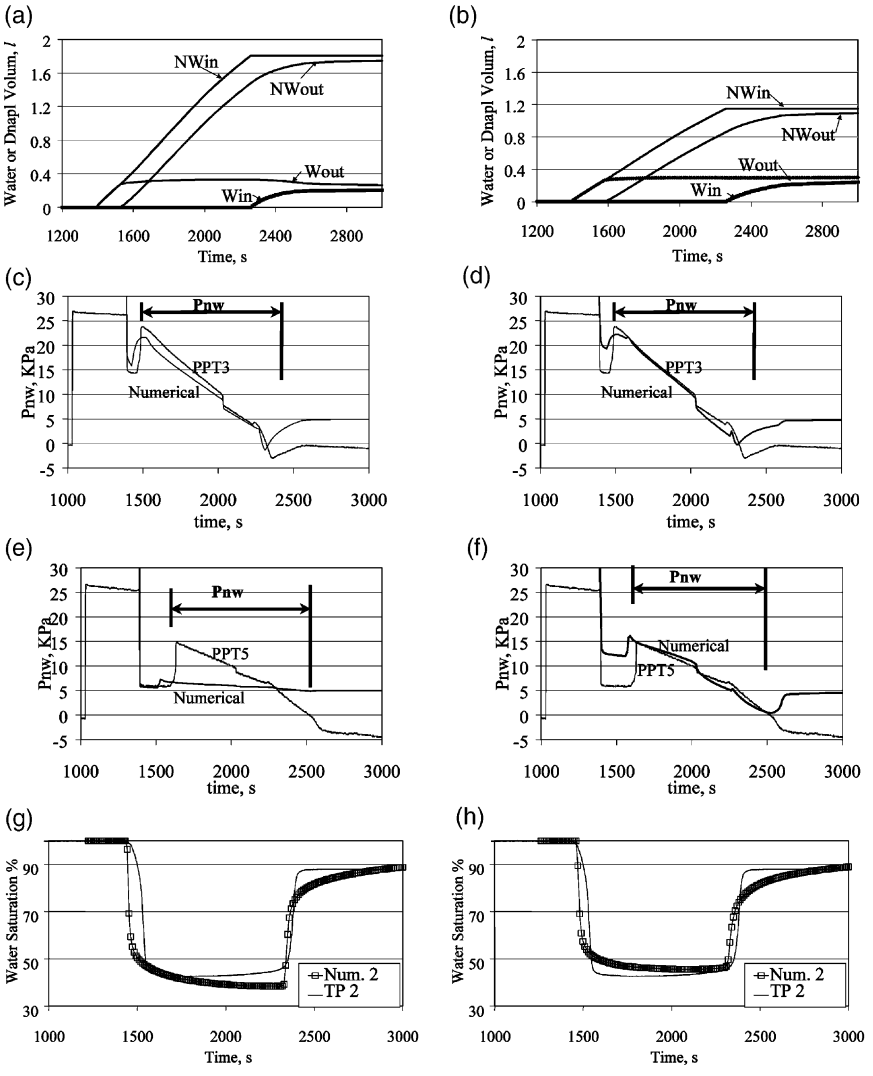

Fig. 9. Experimental and numerical results at 30*g* of (a) accumulated volume of PCE and water inflow and outflow, (b) accumulated volume of PCE and water inflow and outflow for modified simulation, (c) PCE pressure at PPT3, (d) PCE pressure at PPT3 for modified simulation, (e) PCE pressure at PPT5 and (f) PCE pressure at PPT5 for modified simulation, (g) water saturation at TP2, and (h) water saturation at TP2 for modified simulation.

References

Ali, L., Barrufet, M.A., 2001. Using centrifuge data to investigate the effects of polymer treatment on relative permeability. Journal of Petroleum Science and Engineering 29, 1–16.

Ataie-Ashtiani, B., Hassanizadeh, S.M., Celia, M.A., 2002. Effects of heterogeneities on capillary pressure–saturation–relative permeability relationships. Journal of Contaminant Hydrology 56 (3-4), 175–192.

Ataie-Ashtiani, B., Hassanizadeh, S.M., Oostrom, M., Celia, M.A., White, M., 2001. Effective parameters for two-phase flow in a porous medium with periodic heterogeneities. Journal of Contaminant Hydrology 49 (1-2), 87–109.

Ayappa, K.G., Abraham, E.A., Davis, H.T., Davis, E.A., Gordon, J., 1994. Influence of sample width on deducing capillary pressure curves with the centrifuge. Chemical Engineering Science 49 (3), 327–333.

Baldwin, B.A., Spinler, E.A., 1998. A direct method for simultaneously determining positive and negative capillary pressure curves in reservoir rock. Journal of Petroleum Science and Engineering 20, 161–165.

Basha, H.A., Mina, N.I., 1999. Estimation of the unsaturated hydraulic conductivity from the pressure distribution in a centrifugal field. Water Resources Research 35, 469–477.

Brooks, R.H., Corey, A.T., 1964. Hydraulic properties of porous media. Hydrology Paper 3, Civil Engineering Department, Colorado State University, Fort Collins.

Burdine, N.T., 1954. Relative permeability calculations from pore-size distribution data. Petroleum Transactions 198, 71–77.

Depountis, N., Davies, M.C.R., Harris, C., Burkhart, S., Thorel, L., Rezzoug, A., Konig, D., Merrifield, C., Craig, W.H., 2001. Centrifuge modelling of capillary rise. Engineering Geology 60, 95–106.

Garnier, J., et al. 1998. NECER: network of European for environmental geotechnic research: special report. In: Kimura, T., Kusakabe, O., Takemura, J. (Eds.), Centrifuge '98. Balkema, Rotterdam, The Netherlands, pp. 33–55.

Griffioen, J.W., Barry, D.A., 1998. Centrifuge modelling of solute transport during partially saturated flow. Environmental Modelling and Software 14, 191–201.

Illangasekare, T.H., Zniarcic, D., Al-Sheridda, M., Reible, D.D., 1991. Multiphase flow in porous media. In: Ko, H.Y., McLean, F.G. (Eds.), Centrifuge '91. Balkema, Rotterdam, The Netherlands, pp. 517–523.

Johnson, R.L., Pankow, J.F., 1992. Dissolution of dense chlorinated solvents into groundwater II: Source functions for pools or solvent. Environmental Science & Technology 26 (5), 896–901.

Knight, M.A., Mitchell, R.J., 1996. Modelling of light nonaqueous phase liquid (LNAPL) releases into unsaturated sand. Canadian Geotechnical Journal 33 (6), 913–925.

Kueper, B.H., Frind, E.O., 1991. Two-phase flow in heterogeneous porous media 1. Model development. Water Resources Research 27, 1049–1057.

Leverett, M.C., 1941. Capillary behaviour in porous solids. Transactions of American Institute of Mineralogy and Metallurgy Ret. Eng. 142, 152–169.

Marulanda, C., Culligan, P.J., Germaine, J.T., 2000. Centrifuge modeling of air sparging—a study of air flow through saturated porous media. Journal of Hazardous Materials 72, 79–215.

Mitchell, R.J., 1998. The eleventh annual R.M. Hardy Keynote Address: Centrifugation in geoenvironmental practice and education. Canadian Geotechnical Journal 35, 630–640.

Mitchell, R.J., Stratton, B.C., 1994. LNAPL penetration into porous media. In: Leung, C.F., Lee, F.H., Tan, T.S. (Eds.), Centrifuge '94. Balkema, Rotterdam, The Netherland, pp. 345–349.

Mualem, Y., 1976. A new model for predicting the hydraulic conductivity of unsaturated porous media. Water Resources Research 12, 513–522.

Nakajima, H., Hirooka, A., Takemura, J., Marino, M.A., 1998. Centrifuge modeling of one-dimensional subsurface contamination. Journal of the American Water Resources Association 34 (6), 1415–1425.

Nelissen, H.A.M., 1991. The Delft geotechnical centrifuge. In: Ko, H.Y., McLean, F.G. (Eds.), Centrifuge '91. Balkema, Rotterdam, The Netherlands, pp. 35–42.

Oostrom, M., Lenhard, J., 1998. Comparison of relative permeability–saturation–pressure parametric models for infiltration and redistribution of a light nonaqueous phase liquid in sandy porous media. Advances in Water Resources 21, 145–157.

Oostrom, M., Hofstee, C., Dane, J.H., 1997. Light nonaqueous-phase liquid movement in a variably saturated sand. Soil Science Society of America Journal 61, 1547–1554.

Oung, O., Bezuijen, A., 2001. Capillary pressure–saturation curves: experimental determination. GeoDelft report no. DC-750301/350.

Oung, O., Bezuijen, A., Weststrate, F., 2000a. Centrifuge research on the transport of DNAPLs: 1-D flow of a DNAPL through water-saturated sand. In: III Int. Symp. on Physical Modelling and Testing in Environmental Geothenics; La Baule, France., pp. 343–350.

Oung, O., Schenkeveld, F.M., Weststrate, F., 2000b. Centrifuge research on the transport of DNAPLs: the use of dielectric water content sensor to study DNAPL transport in porous media in centrifuge experiments. In: III Int. Symp. on Physical Modelling and Testing in Environmental Geothenics; La Baule, France., pp. 317–324.

Pantazidou, M., Abu-Hassanein, Z.S., Riemer, M.F., 2000. Centrifuge study of DNAPL transport in granular media. Journal of Geotechnical and Geoenvironmental Engineering, ASCE 126 (2), 105–115.

Schroth, M.H., Istok, J.D., Selker, J.S., Oostrom, M., White, M.D., 1998. Multifluid flow in bedded porous media: Laboratory experiments and numerical simulations. Advances in Water Resources 22, 169–183.

van Genuchten, M.Th., 1980. A closed-form equation for predicting the hydraulic conductivity of unsaturated soils. Soil Science Society of America Journal 44, 892–898.

Vaziri, H.H., 1996. Theory and application of a fully coupled thermo-hydro-mechanical finite element model. Computers & Structures 61 (1), 131–146.

White, M.D., Oostrom, M., 1997. STOMP, Subsurface Transport Over Multiple Phases. User's guide. Pacific Northwest National Laboratory Report PNNL-11218.

Zhiang, C.A., Ruth, D.W., 1996. The effect of gravity degradation on low-speed centrifuge capillary pressure data. International Journal of Multiphase Flow 22 (1), 94–98.

Zimmie, T.F., Mahmud, M.B., De, A., 1995. Accelerated physical modelling of radioactive waste migration in soil. International Journal of Rock Mechanics and Mining 32 (6), 260A.